Ultrasound in Med. & Biol., Vol. 40, No. 9, pp. 1980–1990, 2014

0301-5629/$ - see front matter

http://dx.doi.org/10.1016/j.ultrasmedbio.2014.03.010

● *Original Contribution*

AUTOMATIC IDENTIFICATION OF NEEDLE INSERTION SITE IN EPIDURAL ANESTHESIA WITH A CASCADING CLASSIFIER

Shuang Yu,* Kok Kiong Tan,* Ban Leong Sng,† Shengjin Li,‡ and Alex Tiong Heng Sia†
*National University of Singapore, Singapore; †KK Women's and Children's Hospital, Singapore; and ‡Duke–NUS Graduate Medical School, Singapore

(*Received* 9 *October* 2013; *revised* 24 *February* 2014; *in final form* 10 *March* 2014)

Abstract—Ultrasound imaging was used to detect the anatomic structure of lumbar spine from the transverse view, to facilitate needle insertion in epidural anesthesia. The interspinous images that represent proper needle insertion sites were identified automatically with image processing and pattern recognition techniques. On the basis of ultrasound video streams obtained in pregnant patients, the image processing and identification procedure in a previous work was tested and improved. The test results indicate that the pre-processing algorithm performs well on lumbar spine ultrasound images, whereas the classifier is not flexible enough for pregnant patients. To improve the accuracy of identification, we propose a cascading classifier that successfully located the proper needle insertion site on all of the 36 video streams collected from pregnant patients. The results indicate that the proposed image identification procedure is able to identify the ultrasound images of lumbar spine in an automatic manner, so as to facilitate the anesthetists' work to identify the needle insertion point precisely and effectively. (E-mail: yushuang@nus.edu.sg) © **2014 World Federation for Ultrasound in Medicine & Biology.**

Key Words: **Epidural anesthesia, Ultrasound imaging guidance, Automatic identification, Local normalization, Template matching, Cascading classifier, Video processing, Pattern recognition, Medical image processing.**

INTRODUCTION

Epidural anesthesia is a central neuraxial block technique that is widely performed on women during cesarean delivery. This technique is also used to alleviate labor pain. Around 60% to 90% of women in labor receive epidural anesthesia for pain relief (Osterman and Martin 2008). It is rated as one of the most difficult procedures to perform in anesthesiology, with a failure rate of 6%–25% (Konrad et al. 1998; Le Coq et al. 1998; Lewis et al. 1992). A key challenge in manual epidural anesthesia is identification of the needle insertion site, which is determined by palpating the surface landmarks of the spine (Paech et al. 1998). The final needle insertion site can be the result of a trial-and-error process. If the anesthetist feels that the needle is not inserted along the right path, she or he will redirect the needle or withdraw the needle and insert it again at another site. This blind technique can result in multiple insertion attempts, thus compounding the discomfort and distress of patients and decreasing the efficiency of anesthesia.

Since the 1950s, ultrasound imaging has been used in epidural anesthesia to detect the inner anatomic structure of the spine (La Grange et al. 1978). Previous research has confirmed the effectiveness of ultrasound imaging compared with traditional palpation methods (Grau et al. 2002, 2003; Whitty et al. 2008). In practice, ultrasound imaging is used mainly for pre-puncture localization of the needle insertion site before the standard epidural procedure is performed (Arzola et al. 2007; Balki et al. 2009). The ultrasound probe is first positioned in the paramedian orientation to search for the L3–4 spinous level, which is considered the best level for needle insertion; then, the transverse view is employed to search for the precise location of the needle insertion site (Carvalho 2008). A high success rate has also been achieved by researchers who used ultrasound for real-time guidance in the paramedian view (Grau et al. 2004; Karmakar et al. 2009; Tran et al. 2010).

Despite the benefit of pre-puncture localization or real-time ultrasound guidance, one of the key challenges is effective interpretation of the ultrasound image (Ecimovic and Loughrey 2010). Ultrasound images

Address correspondence to: Shuang Yu, Department of Electrical and Computer Engineering, National University of Singapore, Singapore 117576. E-mail: yushuang@nus.edu.sg

contain severe speckle noise, making the subtle structures indistinguishable from surrounding background (Noble et al. 2011). A full interpretation of ultrasound images requires professional training and on-the-job experience. Therefore, although the ultrasound technology is viable, the key challenge remains the accurate interpretation of images in a timely manner. The deep learning curve results in the reluctance of practicing anesthetists to adopt an ultrasound imaging tool on many occasions.

There has been some interest in the applicability of automatic interpretation of ultrasound images, mainly in the paramedian view. Tran and Rohling (2010) used phase symmetry and template matching to extract the lamina and ligamentum flavum in paramedian images. Kerby et al. (2008) proposed labeling the lumbar level automatically with panorama images obtained from the paramedian view. The research was further advanced by Al-Deen Ashab et al. (2013), who developed an augmented reality system (AREA) that projected the identified lumbar vertebra levels on the patients back, to assist spinal needle insertion. Moreover, Al-Deen Ashab (2013) also proposed automatic selection of the optimal paramedian slice plane for needle insertion using the Adaboost algorithm.

Although automatic interpretation of ultrasound images has been explored, the related literature has focused mainly on the paramedian view. There is a paucity of research reports on automatic image interpretation of ultrasound images in the transverse view. The paramedian view is usually employed by practitioners to estimate the L3–4 spinous level. However, for more precise localization of the puncture site, the transverse plane, which reveals reliable landmarks, is preferred by some researchers (Arzola et al. 2007; Balki et al. 2009). In addition, as the majority of anesthetists adopt a midline approach for needle insertion, the importance of the transverse view cannot be over-emphasized (Arzola et al. 2007). The objective of the study described here was to fill the gap in automatic interpretation of ultrasound lumbar spine images in the transverse view for pregnant patients.

In previous research, we developed an image processing and identification procedure for the automatic interpretation of ultrasound images in the transverse view for healthy volunteers (Yu et al. 2013). We proposed combining template matching with a position correlator to identify the interspinous images, and we achieved a success rate of 100% on ultrasound images of the lumbar spine of healthy volunteers. However, because the anatomic features of the lumbar spine might not be clear during pregnancy (Lee et al. 2008), the original position correlator designed for healthy volunteers may not be applicable to pregnant patients. To solve this problem, we improved the identification algorithm and proposed a cascading classifier to improve image identification.

Three main contributions are forthcoming from this study. First, we proposed a cost function based on the appearance of white pixels within a pre-defined window to detect the midline revealed on the ultrasound image, and used a symmetric parameter to ensure the accuracy of midline identification. Second, we improved the image processing and identification procedure with a four-layer cascading classifier for ultrasound image identification. Third, we tested the cascading classifier on ultrasound video streams collected from pregnant patients in an off-line manner. An automatic classification of bone/interspinous frames is described in this article. The epidural space is further automatically identified and measured on interspinous frames with the proposed algorithm.

METHODS

Anatomic structure of lumbar spine

The epidural space is a narrow space located between the ligamentum flavum and dura mater, 3–8 cm below the skin (Palmer et al. 1983), as illustrated in Figure 1. The interspinous spaces between L2 and L3 and between L3 and L4 are most often used for epidural needle insertion for lower limb and abdominal surgery. The largest interspinous spaces are located at those two levels, reducing the difficulty of needle placement compared with that in thoracic interspaces or other lumbar interspinous levels (Halaszynski and Hartmannsgruber 1998). Moreover, the epidural spaces at those two levels are wider, providing

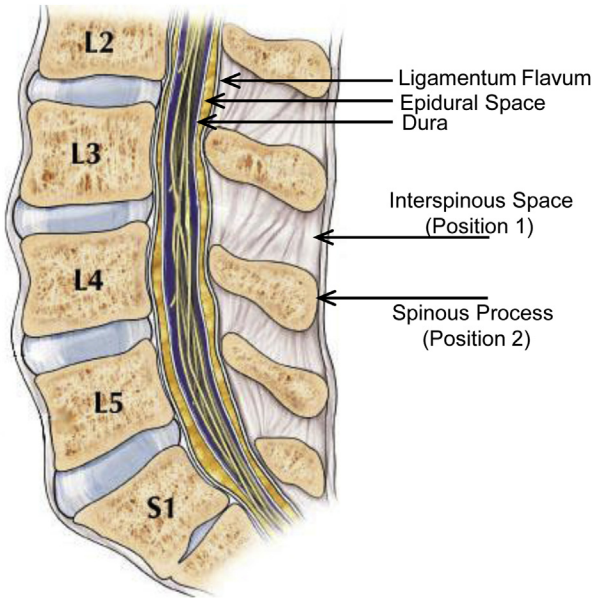

Fig. 1. Lumbar spine anatomy.

the largest safety margin for needle insertion and catheter placement (Bernards 2009; Ebraheim et al. 2004).

Ultrasound image features of lumbar spine

Ultrasound imaging provides anatomic information on 2-D B-mode images corresponding to the plane where the probe is located. As the ultrasound probe is moved, the anatomic structures beneath the probe change accordingly, leading to different image features. When the probe is placed directly on the spinous process, marked as *position 2* in Figure 1, the ultrasound wave is impeded by bones, creating a long triangular hypo-echoic acoustic shadow (Fig. 2a). The midline of the ultrasound image will be dark with a triangular dark window in the middle, which is the main feature of bony images. When the probe is moved to the interspinous region (marked as *position 1* in Fig. 1), more details beneath the skin can be noted (Fig. 2b). The "flying bat"-like shape on the ultrasound image indicates that the location of the probe is a suitable site for needle insertion (Carvalho 2008).

In practice, however, the "flying bat" feature is not easily recognizable, even when the probe is at the best insertion position, because of the poor interpretability of ultrasound images. In our previous research based on ultrasound images obtained in healthy volunteers, we proposed decomposing the "flying bat" feature into three smaller signatory features that represent the interspinous region: the articular processes, the vertebra body and the epidural space. This decomposition allowed detection of the interspinous region 100% of the time in images obtained in healthy volunteers.

Image processing procedure

Speckle is characteristic of ultrasound images, exacerbating the difficulty in interpretation. Tissue attenuation further reduces reflected wave intensity as a function of depth (Martin 2011). To remove speckle and compensate for the effect of attenuation, local normalization enhanced with the difference of Gaussian (DoG) was employed for image pre-processing. After pre-processing, speckle was removed while the main anatomic structures of the ultrasound image were extracted, as illustrated in Figure 3. Local means induced by the non-uniform wave reflection rate were also successfully removed by the pre-processing procedure, eliminating a potential element that might degrade the accuracy of image recognition. (Note: In the DoG step, the optimal Gaussian kernel used for kernel 1 is 20×20 in size [$\sigma = 4$]; and that for kernel 2 is 20×20 [$\sigma = 10$]. For the local normalization step, the optimal Gaussian kernel is the same as kernel 2.)

For the classification of bone images and interspinous images, template matching was employed to search for the best match between signatory features and the original ultrasound images. Three signatory features—the articular process (Fig. 4a) and the epidural space and vertebra body (Fig. 4b)—were used to represent the interspinous space. Positions that corresponded to the signatory features in the images would be maximized in the template matching value, as illustrated in Figure 4(c, d).

To discriminate interspinous images from bone images, a position correlator, which identifies the label of images based on the relative positions of the two matched signatory features, was implemented. The articular process is always located superior to the vertebra body in the ultrasound image, and follows the anatomic structure of the lumbar spine. Only images that satisfy the position correlator were classified as interspinous images; other images were labeled bone images. Template matching with the position correlator worked very well for the ultrasound images obtained in volunteers, with an accuracy rate near 100%. The computational speed achieved was only 0.02 s per image, fast enough for real-time identification.

The image processing and identification procedure is outlined in Figure 5. A detailed illustration can be found in Yu et al. (2013).

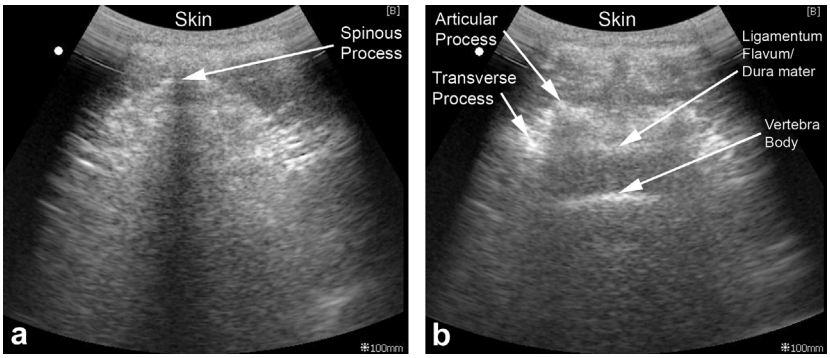

Fig. 2. Ultrasound image of lumbar spine. (a) Typical ultrasound image obtained when the probe is placed above the spinous process; note the triangular anechoic window. (b) Ultrasound image obtained when the probe is placed on the interspinous space.

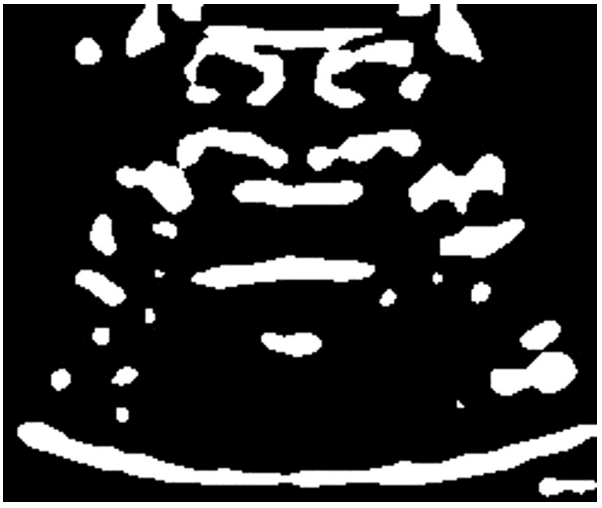

Fig. 3. Pre-processing with difference of Gaussian-modified local normalization.

Improved position correlator

With respect to the ultrasound images collected from volunteers, the original position correlator developed in Yu et al. (2013), which is concerned only with the relative positions of the articular process and vertebra body, achieved a 100% success rate on the 239 ultrasound images. However, the same position correlator performed poorly on the video streams collected from pregnant patients, because the visibility of key anatomic features decreases during pregnancy (Grau et al. 2001). To improve identification accuracy, an improved version of the position correlator that accounts for the anatomic structure of the lumbar spine was developed (Fig. 6).

The matched results for the articular process (the left articular process is represented by $[x_1, y_1]$ and the right by $[x_2, y_2]$) and vertebra body (position $[x_3, y_3]$) must fulfill the following criteria to be identified as interspinous images:

$$\mathrm{Cond}(1) : a(x_1+x_2)/2+b(y_1+y_2)/2+c\approx 0 \quad (1)$$

$$\mathrm{Cond}(2) : -b(x_1-x_2)+a(y_1-y_2)\approx 0 \quad (2)$$

$$\mathrm{Cond}(3) : ax_3+by_3+c\approx 0 \quad (3)$$

$$\mathrm{Cond}(4) : y_3\geq \mathcal{D} \quad (4)$$

$$\mathrm{Cond}(5) : y_3 \gg y_4 \quad (5)$$

$$\mathrm{Cond}(6) : \mathrm{M}\geq \alpha \quad (6)$$

Equations (1) and (2) indicate that the left and right articular processes should be symmetric along the symmetry axis. Equation (3) indicates that the center of the vertebra body should be located on or near the symmetry axis. Equations (4)–(6) indicate that the vertebra body should be located deeper than the articular process and the matching result should be larger than a given threshold α.

Midline detection

To locate the midline, a cost function, $J(\vartheta, x_0)$, based on the summation of weighted pixel values within a predefined window was formulated. The window is scanned through the entire image within $[-45, +45]$ degrees. The

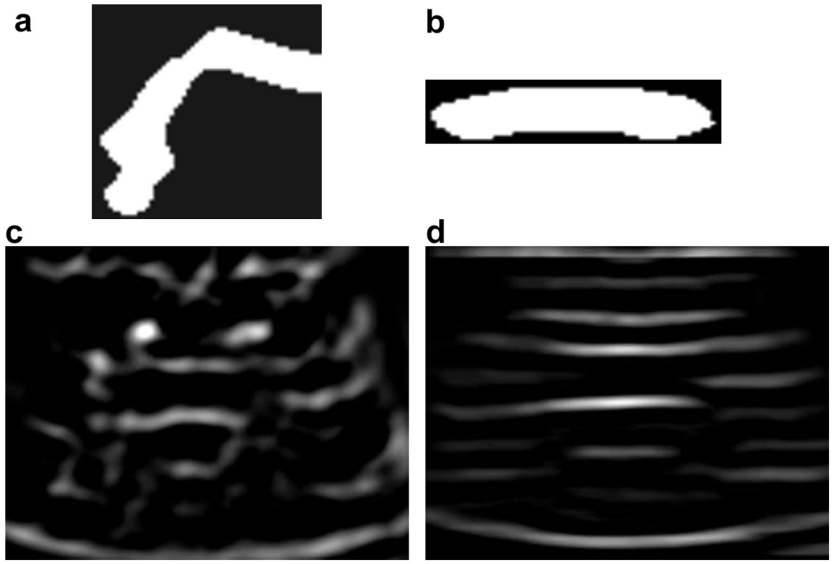

Fig. 4. Ultrasound image processing using template matching. (a) Signatory template for articular process. (b) Signatory template for vertebra body. (c) Matching results for articular process. (d) Matching result for vertebra body.

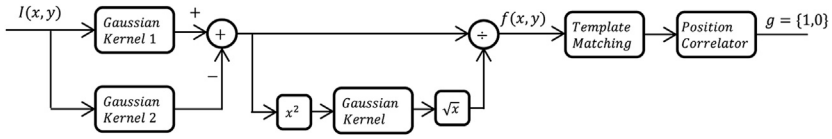

Fig. 5. Image processing flowchart.

position (x_0) and angle (ϑ) that produce the minimal cost are considered to be the midline of the image. This deduction is based on the fact that the bone image yields a dark window near the midline; and for the interspinous image, this holds true most times.

To increase the accuracy of midline detection in interspinous images, a penalty that decreases its weight as a function of depth is imposed on the cost function. Because the vertebra body and epidural space usually appear at the deeper part of the interspinous image, a weight that decreases with depth will allow the appearance of the vertebra body to be penalized less toward the cost function, and thus, the midline location can be calculated with higher accuracy for the interspinous images. Meanwhile, the weight change will not affect the bone images, because in bone images, there are no white pixels (value is 1) along the midline.

$$J(\vartheta, x_0) = \sum_{i=1}^{n} \sum_{j=-C}^{C} [0.5 + exp(-0.1i)] \times f(i, itan\vartheta + x_0 + j) \times \sqrt{(1 + 0.3|\vartheta||x_0 - n/2|)} \quad (7)$$

The cost function J is formulated with two variables, the degree of the line off the vertical direction ϑ and the starting point $(1, x_0)$. The cost function will reduce the penalty if white pixels appear in the deeper part of the image, so that it is still applicable for interspinous images wherein the vertebra body appears near the midline. The last part of the cost function is there to penalize the lines that are not at 0 degree. Because in clinical applications, the midline is required to be in the middle of the image and to be vertical, a penalty is applied if the line is not vertical or in the middle. The pair of parameters ϑ and x_0 that minimize the cost function locate the midline. Note that C denotes the half-size of the pre-defined window, and it is a constant value. The dimensions of the image are denoted as $m \times n$.

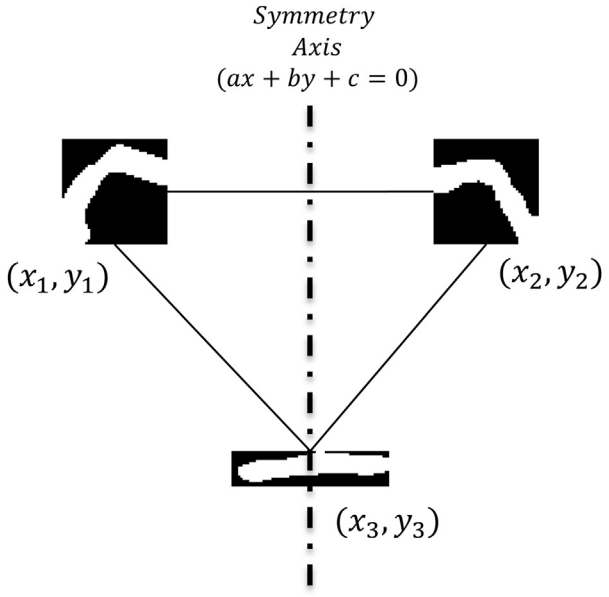

Fig. 6. Improved position correlator.

After the midline is obtained with the above cost function, the dark rate Δ within the pre-defined window is calculated with the equation

$$\Delta = 1 - \frac{\min(J)}{2Cm} \quad (8)$$

Although the use of decreasing weight greatly improves the accuracy of identification of the midline of interspinous images, we found that for certain ultrasound images, an incorrect midline may be identified by the cost function. This often results when the articular process is far from the vertebra body in the horizontal direction. If the horizontal distance is larger than the pre-defined window, then the cost function would be minimized at the gap between the articular process and the vertebra body, rather than at the midline. To rectify this incorrect identification, symmetry detection is employed. The ultrasound images of the lumbar spine should be symmetric along the midline. Therefore, a symmetry indicator can serve as additional confirmation of the identification of the midline using the cost function approach.

Using the cost function to obtain the midline and then using symmetry detection to re-confirm its location improved computational speed and accuracy, compared with an alternate method, that is, full symmetric detection.

The symmetry parameter of the image against the midline detected by the cost function is defined by the equation

$$S = \frac{\sum |f(x,y) - f(x',y')|}{mx_0} \quad (9)$$

where (x, y) and (x', y') represent the coordinates of one pair of pixels which are symmetric against the detected midline.

Midline detection adds another two conditions to the image classification procedure: the symmetric parameter and the dark rate:

$$\text{Cond}(7) : S > \mathcal{S} \tag{10}$$

$$\text{Cond}(8) : \Delta \leq \mathcal{R} \tag{11}$$

In these equations, $\mathcal{S}$ and $\mathcal{R}$ denote the threshold for symmetric parameter S and dark rate Δ, respectively.

Cascading classifier for image classification

The position correlator with midline detection improved the recognition rate in pregnant cases, compared with the original position correlator in Yu et al. (2013). It was able to identify the interspinous images from 21 of the 36 ultrasound video streams, as long as the articular process and vertebra body were both visible. However, among some of the collected pregnant cases, the articular processes were not visible or easily recognizable, and only the vertebra body appeared, even at the best insertion point locations. In those extreme cases, the position correlator would fail to identify the interspinous images.

To strengthen the classifier and make it able to recognize extreme cases, a cascading classifier was developed. The cascading classifier is composed of a series of classifiers so that if the image cannot be confidently classified by a certain classifier, it will be passed to the next classifier, until it is classified with a high confidence level. The structure of the proposed cascading classifier is illustrated in Figure 7.

The first layer of the cascading classifier is the appearance of the vertebra body. The criterion indicates that the vertebra body detector should be maximized at the lower part of the image and close to the symmetry axis. If the first criterion is not met, the image is classified as a bone image; otherwise, it is passed to the second layer. The second layer is the position correlator described in the previous section. If the second criterion is satisfied, then the image is identified as an interspinous image; otherwise, it is passed to the third layer, which classifies images on the basis of the symmetry detection parameter. If the image symmetry parameter along the detected midline is higher than a certain threshold, then the image is classified as an interspinous image. If the criterion at the third layer is not satisfied, then the image is passed to the fourth layer, which computes the maximal dark rate identified by the cost function. If the dark rate is lower than a certain threshold, indicating that there are a considerable number of white pixels within the pre-defined window, then the image is identified as an interspinous image. Otherwise, the image is labeled as a bone image, as there are no further classifier layers.

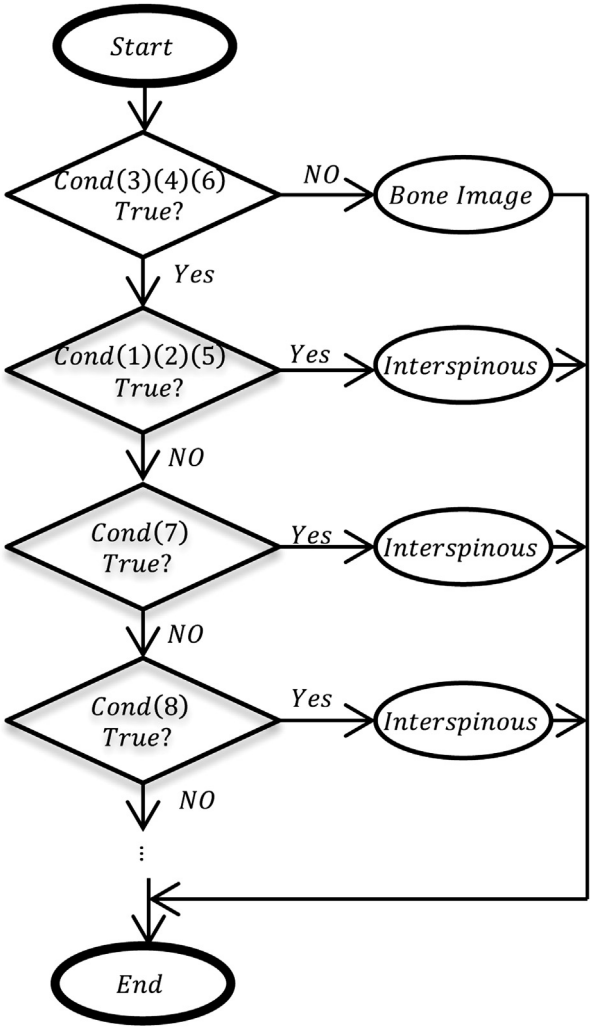

Fig. 7. Cascading classifier.

Identification of epidural space

The epidural space is the target in epidural anesthesia; it is where the needle is placed and medication is delivered. Identification of the epidural space is also an important landmark for spinal needle insertion in spinal anesthesia. The epidural space is visible only on ultrasound images taken from the interspinous region. Once the processed image is identified as an interspinous image with the proposed cascading classifier, it is then possible to search for the epidural space within a certain confine of the image.

The epidural space, according to the anatomic structure of the lumbar spine, is located between the articular process and vertebra body. Moreover, like the vertebra body, the epidural space also appears as a linear feature in ultrasound images. The signatory template used for

vertebra body identification also results in a large matching value at the epidural space, though less than that of the vertebra body, as indicated by the matching results in Figure 8. In certain pregnant patients, the epidural space is more obvious than the vertebra body and the template matching result will maximize at the epidural space instead of at the vertebra body. In such cases, the algorithm will search for the two brightest lines in the matching results and identify the deeper one as the vertebra body and the superior one as the epidural space. Therefore, the epidural space can also be identified from the template matching results of the vertebra body.

Materials and image acquisition

The ultrasound video streams used in this research were collected from KK Women's and Children's Hospital, with institutional review board approval and the patients' consent. Pregnant women scheduled for a caesarean procedure were recruited before they were sent to the operation theater. For data collection, an ultrasound system (Model U660, Canyearn Medical Equipment, Chengdu, China) and a 3.5-MHz curvilinear ultrasound probe (C3.5MHzR60, Canyearn Medical Equipment) were employed, with the scanning depth set to 8–10 cm. The ultrasound video streams were recorded from the lumbar spine in the transverse view (L3–4 or L2–3) at a constant speed of 15 frames per second (FPS) and then saved in Windows Media Video format for processing. The length of the collected video streams ranged from 10 to 20 s, with 150–300 frames obtained from each participant. In total, 36 video streams were recorded for 36 different pregnant patients. The ultrasound video streams were later processed with the described image processing algorithms off-line.

The image processing algorithm was implemented with the MATLAB Computer Vision System toolbox (The MathWorks, Natick, MA, USA) and run on a personal computer (3.3-GHz Core i5-3550 CPU and 8 GB installed memory). Sector images were cropped and downsampled by a factor of 2 to improve the computation speed. An experienced sonographer participated in the research, helping to collect ultrasound video streams and identify whether an image or video frame was suitable for needle insertion, that is, whether the image was an interspinous image or a bone image. The labeling provided by the sonographer was treated as the "gold standard" and then compared with the classification results produced by the algorithm, to evaluate the performance of the algorithm.

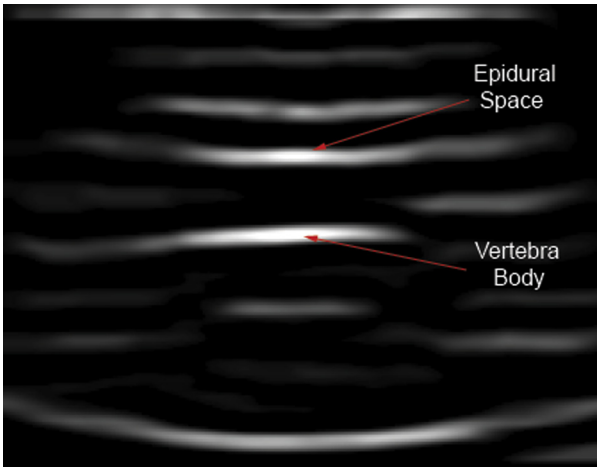

Fig. 8. Identification of epidural space.

RESULTS

There are four parameters ($\mathcal{D}$, α, $\mathcal{S}$ and $\mathcal{R}$) in the cascading classifier that influence the performance of the classifier. To search for the parameters that achieve optimal performance, 20 video streams were randomly selected from the 36 patients and designated as the training set, and the remaining 16 video streams were designated as the test set. From each of the training videos and test videos, 40 images were randomly extracted to evaluate the classifier's performance qualitatively.

Each of the randomly selected ultrasound video frames was labeled by the sonographer as 1 for interspinous images and–1 for bone images. Frames located near the junction of interspinous and bone images were labeled 0, because it was difficult to assign a clear label. The label provided by the sonographer was used to tune the classifier's parameters and evaluate the accuracy of the algorithm. The basic statistics of the training and test set are summarized in Table 1.

Parameters were tuned on the basis of the training set. The parameters that achieved optimal accuracy were chosen as the threshold for the cascading classifier: to $\mathcal{D} = 4.5$ cm, $\alpha = 0.45$, $\mathcal{S} = 0.6$ and $\mathcal{R} = 0.95$. The test results of the cascading classifier with the given parameters are outlined in Table 2.

The proposed cascading classifier was also tested on the 36 video streams, in an attempt to determine the best needle insertion location in real time. Successful identification of a needle insertion site is defined as follows: If the interspinous images appeared continuously, indicating that the probe is placed on the interspinous space, the classifier should be able to identify the interspinous images in at least five consecutive images; whereas if

Table 1. Statistics for the training and test sets

	Training set	Test set
Subjects	20	16
Images	800	640
Non-labeled images	58	26
Interspinous images	448	349
Bone images	294	265

Table 2. Classification results for training and test sets

	Training set	Test set
Accuracy	94.80%	93.23%
Precision	95.90%	93.94%
Recall	95.46%	93.00%
$F_{0.5}$	95.81%	93.75%

the bone images appear continuously in the video streams, then the classifier will not give positive results in more than two continuous frames. The classifier is not required to identify all interspinous frames and bone frames, but those that appear continuously should be correctly identified. Needle insertion points were successfully located on 20 of 20 training videos and 16 of 16 test videos.

An example of related video frames is provided in Figure 9 with the identification results. The circle superimposed on the images indicates that the image was identified as an interspinous image by the algorithm. For case 9(a), the anatomic structures revealed on the image are very clear and the "flying bat" shape is easily recognizable. For cases 9(b) and 9(d), the "flying bat" shape is not as obvious, but is discernable. For cases 9(c) and 9(e), the "flying bat" is hardly visible; however, the appearance of vertebra body indicates that the image is interspinous.

Table 3 lists the computational costs of major functions employed in the image processing procedure. MATLAB (R2012a) was used for implementation of the algorithm. Symmetry detection (18.98 ms) and midline detection (16.99 ms) are the two functions that consumed most of the computational cost (60.07%). It takes 59.9 ms to process one single frame, reaching the computational speed of 16.67 FPS. Given that video streams are collected at a rate of 15 FPS, the algorithm is fast enough for real-time video processing.

Precision and accuracy of epidural space measurement

The visibility of the epidural space can decrease in pregnant women (Grau et al. 2001). This was noted during the present study as well. The epidural space was visible in 31 of the 36 ultrasound video streams. Figure 9(e) illustrates a case where the epidural space was not visible on the interspinous image. For the 31 video streams, the epidural space was measured in two ways: manually by the sonographer and automatically with our algorithm. For the manual measurement, the sonographer chose one frame in which the epidural space was clearly visible and then measured its depth using the caliper function of the ultrasound machine. For automatic measurement, the algorithm first identified the interspinous image continuously and then measured epidural depth as the mean of the epidural depth as it appeared in the interspinous images.

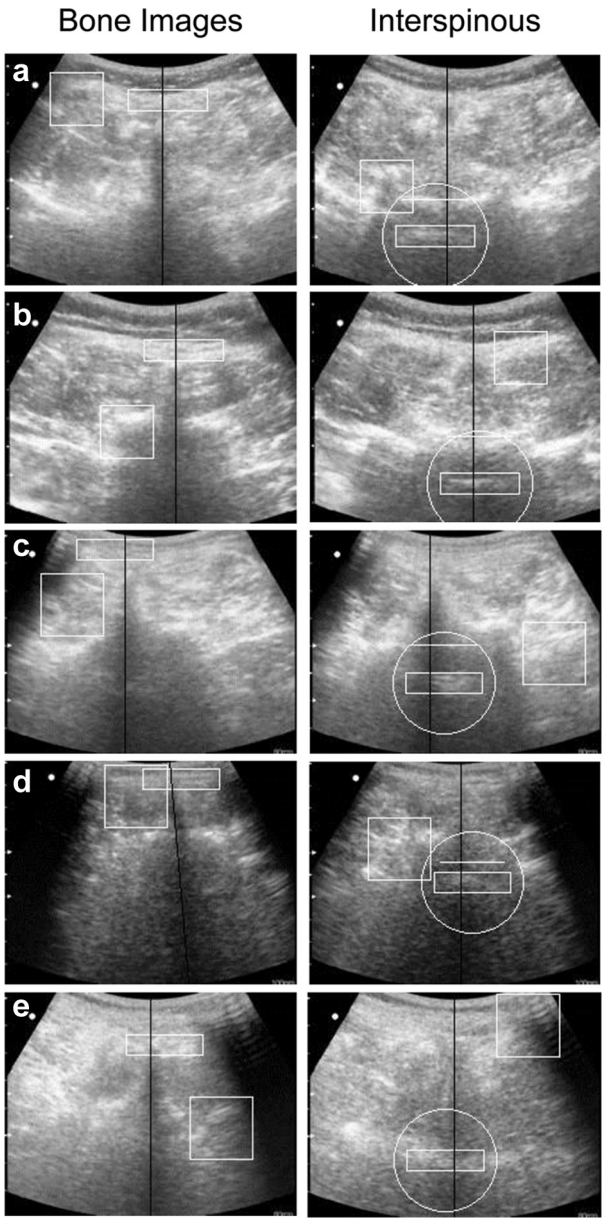

Fig. 9. Identification results for randomly selected video streams. (a) A typical case of 'flying bat' shape interspinous image. (b) and (d), the 'flying bat' shape is not obvious but discernable. (c) and (e), difficult to identify with the 'flying bat' criteria. In the images, the *square box* indicates the matching position for the articular process, and the *rectangle* indicates the position of the vertebra body. In the right column of images, the *circle* indicates it is an interspinous image, and the *white line* above the vertebra body indicates the epidural space identified by the algorithm.

Figure 10(a) illustrates the results for both measurements. Linear regression analysis of the two methods results in the relationship

$$\text{automatic} = 1.016 \times \text{manual} - 0.078 \qquad (12)$$

The coefficient of determination (R^2) is 0.9861 for the linear regression equation, indicating a high, linear

Table 3. Computation costs of functions with MATLAB (image size: 175 × 230)

Function	Computation cost (ms)
Pre-processing: Difference of Gaussian + normalization	9.0
Template matching	13.1
Midline detection	16.99
Symmetry detection	18.98
Cascading classifier	0.029
Processing time per frame	59.9

correlation between manual measurement and automatic measurement. As illustrated in Figure 10(b), the error between automatically measured depth and manually measured depth ranges from –0.128 to 0.15 cm (average = 0.0028 cm, standard deviation = 0.0528 cm, 95% limits of agreement = –0.1008 to 0.1064 cm).

DISCUSSION

The low resolution of ultrasound images and the corresponding decrease in clarity of the subtle anatomic structures pose a challenge in interspinous image identification for the pregnant population, resulting in a low recall rate with the position correlator. The cascading structured classifier developed in this study addresses this problem by using layers of weak classifiers. Important parameters, including matching values and positions of signatory templates, symmetry against midline and black rate within the pre-defined window along midline, serve as weak classifiers to discriminate bone images from interspinous images. The first layer of the cascading classifier ensures the appearance of the vertebra body, which is the basic criterion for identification of images as interspinous images; whereas the continuous layers increase the possibility that interspinous images will be picked up from the imaging pool. Therefore, the cascading classifier achieves a balance between precision and recall, further increasing the accuracy of identification.

The error of intra-observer repeatability of ultrasound imaging measurement was reported to range from 4.75% to 7% (Balint and Sturrock 2001). Given that the average measured epidural depth is 4.727 cm in this study, the error of manual measurement of epidural depth may fluctuate between 0.2245 and 0.3309 cm, which is higher than the difference between automatic and manual measurements. Therefore, the automatic measurement is acceptable compared with the manual measurement.

In the image processing procedure, the incorporation of pre-processing alleviates the negative influence

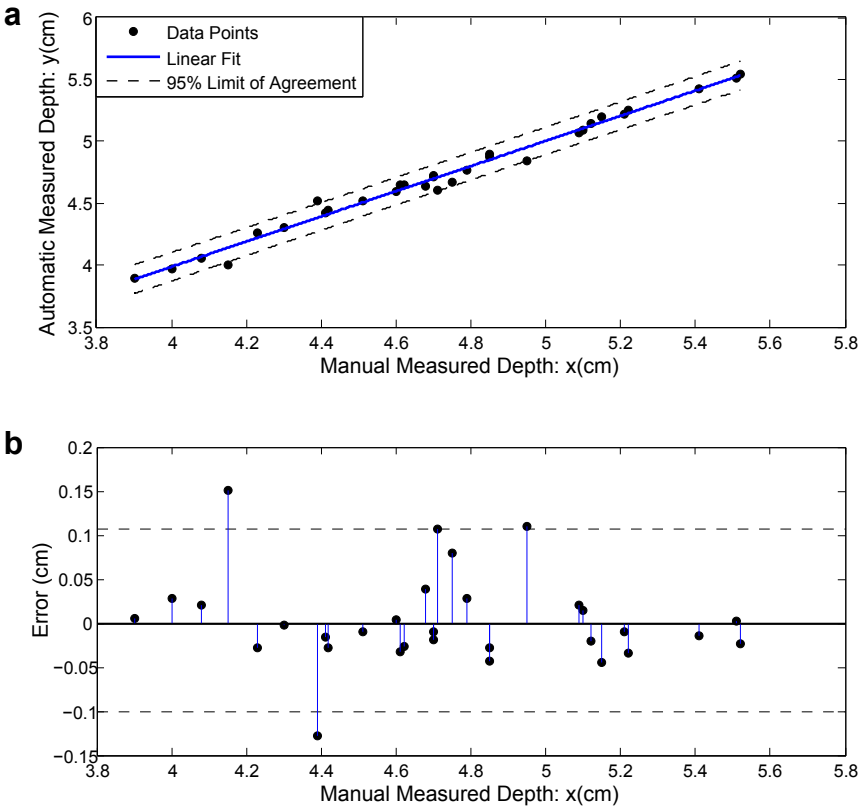

Fig. 10. Comparison of automatically and manually measured epidural Depths. (a) Scatterplot. (b) Differences between automatic measurement and manual measurement.

of image quality on the recognition result. The quality of ultrasound images generally depends on the experience of the sonographer and the proper setting of machine parameters, for example, contrast and gain. Pre-processing using DoG-enhanced local normalization mitigates the dependence of classifier performance on good image quality. After pre-processing, the divergence of image intensity induced by contrast and gain is filtered, increasing robustness. In the cases illustrated in Figure 9, the gain parameter in case (d) was set at 67 in case (d) and at 80 in the remaining cases, leading to different image intensities. Nevertheless, the algorithm successfully identified all of the cases regardless of the difference in image intensity. Thus, anesthetists can use the ultrasound system for epidural needle insertion without extensive knowledge of machine parameter settings and image interpretation.

Although it is not necessary for the operator to tune the optimal contrast and gain parameter to obtain the best image quality, the proper scanning depth must still be chosen. The size of anatomic structures revealed on the ultrasound image will differ with different scanning depths, influencing the optimal choice of Gaussian kernels. If the depth is set excessively deep, then the anatomic structures will be very small and a large Gaussian kernel will filter the tiny anatomic structure as noise, which is not desired. Because the epidural space is usually 3–8 cm below the skin and the vertebra body is 1–2 cm deeper than the epidural space, the proper scanning depth is suggested to be around 8–10 cm. During data collection, the depth was set between 8 and 10 cm and the two Gaussian kernels remained unchanged for all videos. The chosen Gaussian kernels were able to pre-process the raw ultrasound images properly with minor change in scanning depth.

Midline detection is another important feature of the video processing procedure. It not only provides the dark rate, Δ, for the cascading classifier, but also effectively detects the angle and position of the ultrasound probe against the spine midline. In the real-time procedure, a reference line that is vertical and corresponds to the middle of the probe can be superimposed on the image window, so that the operator can be guided to align the detected midline with the reference line. Therefore, while the cascading classifier locates the proper plane for needle insertion, midline detection will locate the spine midline, and the combination of the two techniques can locate the precise insertion point.

We envision the clinical workflow with the developed algorithm as follows: (i) With an ultrasound system running the algorithm in the background in real time, the operator holds the ultrasound probe in the transverse plane, moving it along the patient's midline slowly until a set of continuous interspinous images are detected. (ii) At this point, the operator is prompted to adjust the angle and position of the probe until the detected midline is aligned with the reference line. (iii) When alignment is accomplished, the location of the center of the ultrasound probe will correspond to the proper needle insertion point.

CONCLUSIONS

We have described an image processing and identification procedure for automatic interpretation of ultrasound lumbar spine images in the transverse plane. An initially proposed position correlator was strengthened by using a cascading classifier approach. It includes a cost function based on the minimal appearance of white pixels to locate the midline of the ultrasound image and a symmetric indicator to ensure the accuracy of the midline detection. This enhanced classifier effectively identified the interspinous images with four layers of weak classifiers and successfully located the proper needle insertion point in the 36 pregnant cases collected so far.

The automatic identification of interspinous images and bone images has been realized with the proposed algorithm. In the near future, the interpretation of ultrasound lumbar images will be realized in an automatic and real-time manner by computers, so that anesthetists will not be required to read ultrasound images that are not easily interpretable. It is expected that the use of the ultrasound system can be as easy as a direct sensor for needle site indicator, with our image processing and classification algorithms working in the background in real time. The difficulty associated with epidural needle insertion can thus be potentially alleviated by this approach.

REFERENCES

Al-Deen Ashab H. Ultrasound guidance for epidural anesthesia. Master's thesis, University of British Columbia, Vancouver, 2013.

Al-Deen Ashab H, Lessoway VA, Khallaghi S, Cheng A, Rohling R, Abolmaesumi P. An augmented reality system for epidural anesthesia (AREA): Prepuncture identification of vertebrae. IEEE Trans Biomed Eng 2013;60:2636–2644.

Arzola C, Davies S, Rofaeel A, Carvalho JC. Ultrasound using the transverse approach to the lumbar spine provides reliable landmarks for labor epidurals. Anesth Analg 2007;104:1188–1192.

Balint PV, Sturrock RD. Intraobserver repeatability and inter-observer reproducibility in musculoskeletal ultrasound imaging measurements. Clin Exp Rheumatol 2001;19:89–92.

Balki M, Lee Y, Halpern S, Carvalho JC. Ultrasound imaging of the lumbar spine in the transverse plane: The correlation between estimated and actual depth to the epidural space in obese parturients. Anesth Analg 2009;108:1876–1881.

Bernards CM. Handbook of clinical anesthesia. Philadelphia: Lippincott Williams & Wilkins; 2009.

Carvalho JC. Ultrasound-facilitated epidurals and spinals in obstetrics. Anesthesiol Clin 2008;26:145–158.

Ebraheim NA, Hassan A, Lee M, Xu R. Functional anatomy of the lumbar spine. Semin Pain Med 2004;2:131–137.
Ecimovic P, Loughrey JP. Ultrasound in obstetric anaesthesia: A review of current applications. Int J Obstet Anesth 2010;19:320–326.
Grau T, Bartusseck E, Conradi R, Martin E, Motsch J. Ultrasound imaging improves learning curves in obstetric epidural anesthesia: A preliminary study. Can J Anaesth 2003;50:1047–1050.
Grau T, Leipold RW, Fatehi S, Martin E, Motsch J. Real-time ultrasonic observation of combined spinal-epidural anaesthesia. Eur J Anaesthesiol 2004;21:25–31.
Grau T, Leipold RW, Conradi R, Martin E, Motsch J. Efficacy of ultrasound imaging in obstetric epidural anesthesia. J Clin Anesth 2002; 14:169–175.
Grau T, Leipold RW, Horter J, Conradi R, Martin E, Motsch J. The lumbar epidural space in pregnancy: Visualization by ultrasonography. Br J Anaesth 2001;86:798–804.
Halaszynski TM, Hartmannsgruber MWB. Anatomy and physiology of spinal and epidural anesthesia. Semin Anesth Periop Med Pain 1998; 17:24–37.
Karmakar MK, Li X, Ho AM, Kwok WH, Chui PT. Real-time ultrasound-guided paramedian epidural access: Evaluation of a novel in-plane technique. Br J Anaesth 2009;102:845–854.
Kerby B, Rohling R, Nair V, Abolmaesumi P. Automatic identification of lumbar level with ultrasound. Conf Proc IEEE Eng Med Biol Soc 2008;2008:2980–2983.
Konrad C, Schüpfer G, Wietlisbach M, Gerber H. Learning manual skills in anesthesiology: Is there a recommended number of cases for anesthetic procedures. Anesth Analg 1998;86:635–639.
La Grange P, Foster PA, Pretorius LK. Application of the Doppler ultrasound blood flow detector in supraclavicular brachial plexus block. Br J Anaesth 1978;50:965–967.
Le Coq G, Ducot B, Benhamou D. Risk factors of inadequate pain relief during epidural analgesia for labour and delivery. Can J Anaesth 1998;45:719–723.
Lee Y, Tanaka M, Carvalho JC. Sonoanatomy of the lumbar spine in patients with previous unintentional dural punctures during labour epidurals. Reg Anesth Pain Med 2008;33:266–270.
Lewis MP, Thomas P, Wilson LF, Mulholland RC. The 'whoosh' test. A clinical test to confirm correct needle placement in caudal epidural injections. Anaesthesia 1992;47:57–58.
Martin K. Basic equipment, components and image production. In: Allan PL, Baxter GM, Weston MJ, (eds). Clinical Ultrasound. Elsevier Health Sciences UK; 2011. p. 16–30.
Noble JA, Navab N, Becher H. Ultrasonic image analysis and image-guided interventions. Interface Focus 2011;1:673–685.
Osterman MJK, Martin JA. Epidural and spinal anesthesia use during labor: 27-State reporting area. Atlanta, GA: Centers for Disease Control and Prevention; 2008.
Paech MJ, Godkin R, Webster S. Complications of obstetric epidural analgesia and anaesthesia: A prospective analysis of 10,995 cases. Int J Obstet Anesth 1998;7:5–11.
Palmer SK, Abram SE, Maitra AM, von Colditz JH. Distance from the skin to the lumbar epidural space in an obstetric population. Anesth Analg 1983;62:944–946.
Tran D, Kamani AA, Al-Attas E, Lessoway VA, Massey S, Rohling RN. Single-operator real-time ultrasound-guidance to aim and insert a lumbar epidural needle. Can J Anaesth 2010;57:313–321.
Tran D, Rohling RN. Automatic detection of lumbar anatomy in ultrasound images of human patients. IEEE Trans Biomed Eng 2010; 57:2248–2256.
Whitty R, Moore M, Macarthur A. Identification of the lumbar interspinous spaces: Palpation versus ultrasound. Anesth Analg 2008;106: 538–540.
Yu S, Tan KK, Shen CY, Sia ATH. Ultrasound guided automatic localization of needle insertion site for epidural anesthesia. In: Proceedings, IEEE International Conference on Mechatronics and Automation, Takamatsu, Japan, August 4–7, 2013: 985–990.